

# RSC Advances



This is an *Accepted Manuscript*, which has been through the Royal Society of Chemistry peer review process and has been accepted for publication.

*Accepted Manuscripts* are published online shortly after acceptance, before technical editing, formatting and proof reading. Using this free service, authors can make their results available to the community, in citable form, before we publish the edited article. This *Accepted Manuscript* will be replaced by the edited, formatted and paginated article as soon as this is available.

You can find more information about *Accepted Manuscripts* in the [Information for Authors](#).

Please note that technical editing may introduce minor changes to the text and/or graphics, which may alter content. The journal's standard [Terms & Conditions](#) and the [Ethical guidelines](#) still apply. In no event shall the Royal Society of Chemistry be held responsible for any errors or omissions in this *Accepted Manuscript* or any consequences arising from the use of any information it contains.



## Tungsten Carbide/Iron Sulfide/FePt Nanocomposite Supported on Nitrogen-doped Carbon as an Efficient Electrocatalyst for Oxygen Reduction Reaction

Zesheng Li,<sup>\*a</sup> Bolin Li,<sup>a</sup> Zhisen Liu,<sup>a</sup> Zhenghui Liu<sup>a</sup> and Dehao Li<sup>a</sup>

Received 00th January 20xx,  
Accepted 00th January 20xx

DOI: 10.1039/x0xx00000x

www.rsc.org/

- The development of multi-component electrocatalysts offers great promise to enhance catalytic performances for the oxygen reduction reactions (ORR) of fuel cells. Herein, we report a novel hybrid material consisting of multiple components of tungsten carbide (WC), iron sulfide (FeS), FePt and nitrogen-doped carbon (NC), i.e. WC/FeS/FePt/NC hybrid architecture, as a high-performance electrocatalyst for the ORR. Due to the attractive multiple promoting effects from these components, the present Pt-based electrocatalyst exhibits excellent mass activity of 317 mA mg<sup>-1</sup> Pt (at 0.9 V vs. RHE), which is about 2.5 times as high as that of commercial Pt/C catalyst (125 mA mg<sup>-1</sup> Pt). Moreover, superior durability in acidic electrolyte of the WC/FeS/FePt/NC is also demonstrated for the ORR. Importantly, this work provides a new thought for the design of high-performance ORR electrocatalysts by integrating the promoting effects of multiple components (especially for carbides and sulphides) on noble metals, which presents promising potential application for fuel cells.

### 1. Introduction

Nowadays, proton exchange membrane fuel cells (PEMFCs) have attracted considerable and persistent attention for both transportation and stationary power applications advantaged from their high energy conversion efficiency, low operation temperature, as well as low pollution emissions.<sup>1</sup> It is common known that Platinum (Pt)-based noble metal catalysts are still one of best candidates in the practical application of PEMFCs.<sup>2</sup> However, developing cost-effective Pt-based catalysts for oxygen reduction reaction (ORR) at the cathode of PEMFCs is a severe technological bottleneck. Because the present Pt-based catalysis is confronted with three important problems, including heavy Pt-dependence,<sup>3</sup> sluggish ORR kinetics,<sup>4</sup> and limited durability,<sup>5</sup> which have produced deadly influence on the efficiency of PEMFCs and their economic benefit. Therefore, it is of fundamental interest to develop low-Pt-loading, highly efficient and durable ORR electrocatalysts for the sake of the popularization and application of PEMFCs.<sup>6</sup>

It has been well demonstrated that the noble metal nanoparticles supported on or around metal carbides (e.g. WC<sub>x</sub>, MoC<sub>x</sub>, VC<sub>x</sub>, etc.) could perform significantly enhanced ORR kinetics owing to the

well-known synergistic effects.<sup>7</sup> The enhancement of WC on Pt metal has been widely demonstrated for ORR catalysis, in which the WC as electrocatalyst promoter could greatly improve the catalytic activity of Pt metal, originated from the electron-donating effect of tungsten species.<sup>8</sup> To achieve the optimized synergistic effect, the constitutive uniformity and dimensional controllability of WC appear to be the essential requirements.<sup>9</sup> Apparently, uniform distributions and small particle sizes can endow WC with maximum utilization efficiency and higher synergistic catalytic activity.<sup>10</sup> For this purpose, great research efforts have recently been focused on the size controlling of WC nanoparticles. For example, He et al. reported the synthesis of WC nanoparticles in size of 10 nm on carbon by an intermittent microwave heating method, which showed a high ORR catalytic activity of 207.4 mA mg<sup>-1</sup> Pt at 0.9V.<sup>11</sup> Recently, Shen and co-workers further developed WC nanoparticles less than 2 nm on carbon by an ion-exchange and Fe-mediated method, which showed a higher ORR catalytic activity of 257.7 mA mg<sup>-1</sup> Pt at 0.9V.<sup>12</sup> However, it should be noted that the single WC-promoted strategy lead to a limited improvement in ORR catalytic activity for Pt metal, in spite of their ultra-tiny diameter of WC nanoparticles.<sup>13</sup> Therefore, the multi-component promoting strategy should be proposed, aiming to more outstanding catalytic activity of Pt metal for the ORR.

On the other hand, metal chalcogenides are attracting significant attention in a variety of energy storage and conversion including fuel cells, solar cells, Li-ion batteries, and supercapacitors.<sup>14</sup> Particularly, some of the metal chalcogenides (e.g. CoSe<sub>x</sub>, CoS<sub>x</sub>, FeS<sub>x</sub>, etc.) are expected to serve as effective substitutes to Pt metal for the ORR, as very promising non-precious metal catalysts.<sup>15</sup> For example, cobalt sulphides such as Co<sub>3</sub>S<sub>4</sub> and Co<sub>9</sub>S<sub>8</sub> are rather active for four-electron ORR in acidic electrolytes.<sup>16</sup> A novel CoSe<sub>2</sub>-based catalyst recently showed an onset potential of 0.71 V for the ORR in 0.5 mol H<sub>2</sub>SO<sub>4</sub> electrolyte.<sup>17</sup> Particularly, the Co<sub>1-x</sub>Se and FeS<sub>x</sub> thin-film catalysts

<sup>a</sup> Development Center of Technology for Petrochemical Pollution Control and Cleaner Production of Guangdong Universities, College of Chemical Engineering, Guangdong University of Petrochemical Technology, Maoming, Guangdong, 525000, China.

Corresponding authors  
E-mail addresses:  
<sup>\*</sup> Zesheng Li, lz5212@163.com

† Footnotes relating to the title and/or authors should appear here. Electronic Supplementary Information (ESI) available: [details of any supplementary information available should be included here]. See DOI: 10.1039/x0xx00000x

showed higher ORR activities and stabilities in acidic electrolytes.<sup>18</sup> However, the catalytic activities of these materials are much lower than that of commercial Pt-based catalysts, which needs to be further enhanced for practical fuel cell applications.<sup>19</sup> Fortunately, the ORR catalytic activity of these metal chalcogenides could be effectively enhanced via introducing extraneous functional components, such as Fe<sub>3</sub>O<sub>4</sub> and Pt nanoparticles, due to the potential synergistic effects.<sup>20</sup> Nevertheless, the multi-component hybrid system made up of metal carbides, metal chalcogenides as well as noble metals has not been reported up to now.

Recent studies have demonstrated that MPt bimetallic catalysts (M = Fe, Co, Ni, etc.) are highly active catalysts for the ORR in fuel cell applications.<sup>21</sup> With regard to FePt alloys, for example, the higher ORR activity and durability can be accessible, since the involvement of Fe species could endow Pt with profitable electronic structure and offer a stable intermetallic M-Pt arrangement.<sup>22</sup> On the other hand, compared to bare FePt catalysts, carbon-supported ones have been demonstrated to be more active in ORR catalytic actions, due to the skeleton stabilization and improved charge transport.<sup>23</sup> Remarkably, several important reports suggested that nitrogen-doped carbon can achieve much increased activity for ORR catalysts under harsh fuel cell operating conditions.<sup>24</sup> Particularly, the fascinating synergistic effects have been demonstrated for the ORR when nitrogen-doped carbon is coupled with foreign components.<sup>25</sup> With this in mind, it is highly expected that efficient catalyst for the ORR can be achieved by integrating FePt alloys and promoted components onto nitrogen-doped carbon.

In this investigation, we present a novel multi-component hybrid system, WC/FeS/FePt nanocomposite supported on nitrogen-doped carbon (NC), as an efficient electrocatalyst for the ORR. To the best of our knowledge, this is the first report on the integration of a metal carbide, metal sulfide and Pt-based alloy on to NC, in the interest of a superior catalytic activity of Pt metal. For this hybrid system, three features have become apparent over previous reports: (i) unique 1D WC nanorods with ultra-tiny diameter of 2 nm are harvested by the present synthetic strategy; (ii) FePt alloy is fabricated by the in-situ growth from FeS nanocrystals without additional Fe source; (iii) the dual promoting effects on Pt metal might be in operation relying on WC and FeS components. With these merits, we demonstrate that the ORR electrocatalysts with high performances can be designed by this WC/FeS/FePt/NC hybrid system.

## Experimental

### Synthesis of materials

The macroporous acrylic-type anion-exchange resin (D314) with amidogen groups was used as the carbon and nitrogen sources for the synthesis of WC/FeS/NC hybrid sample, by using the associated ion-exchange process and subsequent sintering process. In a typical synthesis, 20 g of anion-exchange resin (D314) was exchanged with 1,000 mL of aqueous solution which contains 0.1 mol of ammonium metatungstate hydrate ((NH<sub>4</sub>)<sub>6</sub>H<sub>2</sub>W<sub>12</sub>O<sub>40</sub>), 0.05 mol of potassium ferrocyanide (K<sub>4</sub>Fe(CN)<sub>6</sub>) and 0.2 mol of Sodium sulphate (Na<sub>2</sub>SO<sub>4</sub>). The resulting resin/anion complex was then sintered at 900 °C for 2 h under a pure Ar flow. The product was crushed into fine powders by mechanical milling. FeS/NC sample was prepared by using the

same procedures above at the absence of (NH<sub>4</sub>)<sub>6</sub>H<sub>2</sub>W<sub>12</sub>O<sub>40</sub>. In addition, WC/FeS/FePt/NC hybrid catalyst was synthesized by the Intermittent Microwave Heating (IMH) method. Appropriate amount of H<sub>2</sub>PtCl<sub>6</sub> and WC/FeS/NC were mixed with ethylene glycol in an ultrasonic bath for 30 min. The mixture was subjected to microwave heating (5 s on and 5 s off for 20 cycles) using a homemade microwave oven (2,000 W, 2.45 GHz). The product was acidified, filtered, washed and dried at 80 °C for 12 h in vacuum.

### Characterization of materials

The X-ray diffraction (XRD) measurement was carried out with a Bluker D8-Advance diffractometer with Cu K $\alpha$  radiation ( $\lambda = 1.5406 \text{ \AA}$ ). The morphologies of the samples were examined by using a field emission scanning electron microscopy (SEM, Philips, FEI Quanta 200FEG) and a transmission electron microscopy (TEM, JEOL-2010). The X-ray photoelectron spectroscopy (XPS) measurements were carried out on an XPS apparatus (ESCALAB 250).

### Electrochemical measurements

The catalytic activities of the electrocatalysts for the ORR were evaluated by using a Rotating Ring Disc Electrode (RRDE) with a biopotentiostat (AFCBP1E, Pine Instrument Co., USA) at 25 °C with Pt foil as counter electrode and reversible hydrogen electrode (RHE) as reference electrode. A mixed solution of 5.0 mg electrocatalysts, 0.95 mL ethanol and 0.05 mL Nafion solution (0.05 wt %) was ultrasonicated for to form a well-dispersed ink. A certain amount of the ink was transferred onto the surface of the glass carbon in RRDE to be working electrodes. The mass activities of the Pt-based catalyst were calculated from the ORR data by using the mass transport correction for a rotating disk electrode:  $i_k = i_d / (i_d - i)$ , where  $i$  is the experimentally obtained current,  $i_d$  refers to the measured diffusion-limited current and  $i_k$  the mass-transport-free kinetic current. The Chronoamperometric technique was selected to evaluate the electrochemical stability of the as-prepared catalyst samples.

## Results and discussion

The crystallographic structures of the as-prepared samples have been investigated by XRD, and the resultant patterns are shown in Fig. 1. Fig. 1 A demonstrates the wide-angle patterns attained at a scan rate of 10 ° min<sup>-1</sup>, for the FeS/NC, WC/FeS/NC and WC/FeS/FePt/NC. For FeS/NC, the diffraction peaks at 29.9°, 33.6°, 43.2°, 53.1°, and 70.8° correspond to the (100), (101), (102), (110) and (202) planes of FeS phase (JCPDS, 65-6841).<sup>26</sup> For WC/FeS/NC, the additional diffraction peaks at 31.5°, 35.7°, 48.3°, 64.1°, and 73.2° correspond to the (001), (100), (101), (110) and (111) planes of WC phase (JCPDS, 65-8828).<sup>27</sup> It is noteworthy that, different from previously reported WC,<sup>8-13</sup> the WC in WC/FeS/NC sample exhibits a narrower diffraction peak of (100) plane, while broader diffraction peaks of the other planes. The crystallite sizes for the diffraction peaks of (100), (101) and (110) planes were calculated to be 7.5, 3.1 and 4.2 nm, respectively, according to the Scherer equation.<sup>28</sup> These results suggest that the as-prepared WC possesses 1D crystalline structures along the direction of (100) plane. For WC/FeS/FePt/NC, the new diffraction peaks at 40.5°, 47.3°, 69.1° and 83.2° correspond to the (111), (200), (220) and (311) planes of FePt phase (JCPDS, 65-9122).<sup>29</sup> The prominent diffraction peak at 40.5° of the sample is

due to the high diffraction intensity of the (111) plane for the FePt alloy, which is in well accordance with many previous literatures.<sup>30</sup> The crystallite size of the FePt is calculated to be 3.0 nm based on (111) diffraction peak. The diffraction peaks of WC phase (marked by four-angle stars) can be observed in WC/FeS/FePt/NC, while the FeS phase is difficult to identified, due to its reduced content during the growth of FePt alloy. On the other hand, Fig. 1 B demonstrates the selected-angle patterns between 36° and 44° at a scan rate of 2° min<sup>-1</sup>. It is obvious that the diffraction peak of FePt (111) is shifted to a higher 2θ value (40.5°) compared with that (39.8°) of the Pt (111) (for the commercial Pt/C catalyst, TKK, 46.7% Pt), indicating that partial Fe atoms from FeS has entered into the Pt lattice and the FePt alloy has formed.<sup>31</sup>

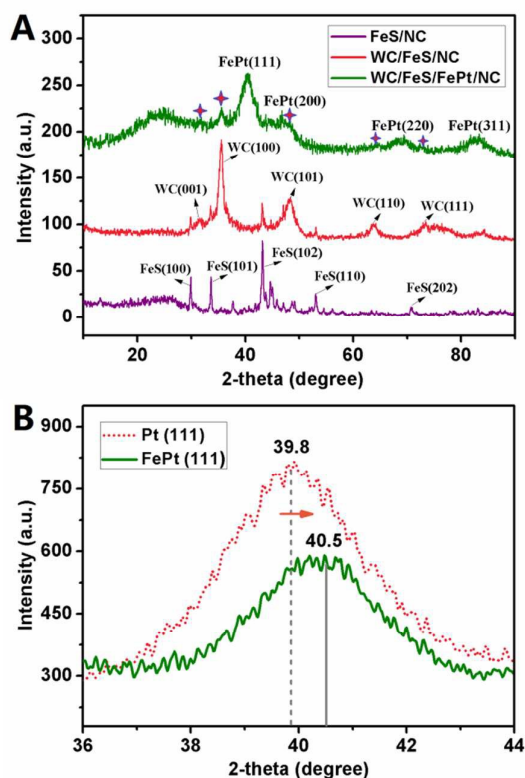


Fig. 1 (A) XRD patterns of the as-prepared samples and (B) selected-angle patterns of Pt (111) and FePt (111).

The morphology of the WC/FeS/FePt/NC architecture was further observed by SEM. And the chemical composition of the sample was determined by the EDS attached to SEM. Fig. 2 reveals the typical SEM images of WC/FeS/FePt/NC sample. It is obvious that the sample has a well-dispersed nanoparticles structure with about 100 nm in sizes. These nanoparticles can be assigned to the NC, and the latent WC/FeS/FePt species are supported on them. It is noteworthy to note that a well-dispersed supported system is highly desirable for reaching outstanding catalytic performances. Fig. 3 displays the EDS pattern and SEM-EDS mapping images of WC/FeS/FePt/NC sample. The components of this sample are showed in Fig. 3 A, which suggests the presence of C, O, N, S, W, Fe and Pt elements in the composite. The contents of these elements are also presented by the inserted table in Fig. 3 A. Obviously, C is one dominant element

corresponding to the NC and WC. The elements of O and N come from the oxygen containing groups and amidogen groups of the resin precursor, respectively. The content of N in the sample is 0.57 % in atomic percent that might be a trace-doping into the NC. In addition, the content of Pt in the sample is 28.38 % in weight percent, which indicates that the Pt metal has been deposited onto the surface of NC. The atomic ratio of Fe and S is about 1.55 that is higher than the predicted one (1.00) of FeS in stoichiometry. This result further demonstrates that partial Fe atoms in FeS entered into the Pt metal to form FePt alloy, being in well accordance with the finding of XRD. On the other hand, the SEM-EDS mapping images in Fig. 3 B shows that these elements of C, O, N, S, W, Fe and Pt are homogeneously distributed on the sample within a large mapping range. A favorable constitutive uniformity is fairly important to maximize the catalytic activity of hybrid system.

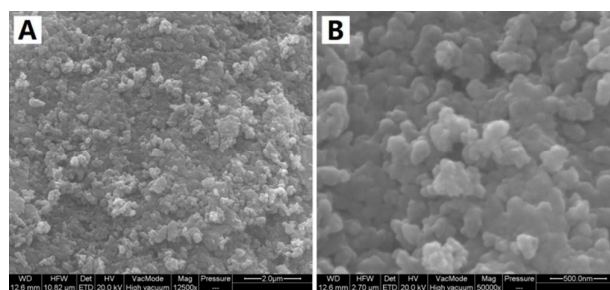


Fig. 2 Typical SEM images of the WC/FeS/FePt/NC sample.

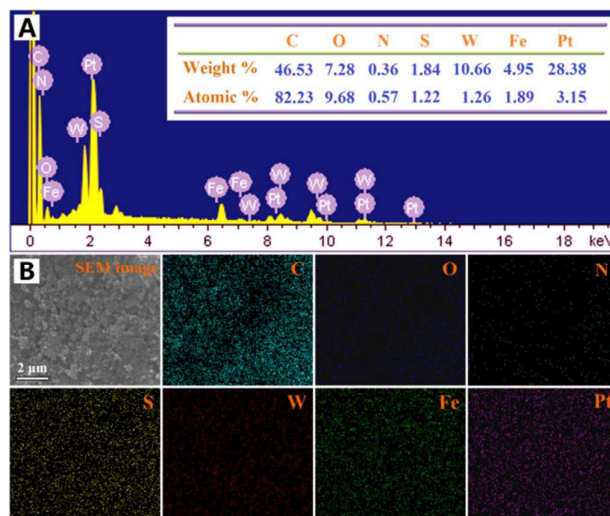


Fig. 3 EDS pattern (including element contents) (A) and SEM-EDS mapping images (B) of the WC/FeS/FePt/NC sample.

Fig. 4 shows typical TEM images of the WC/FeS/FePt/NC hybrid architecture. From Fig. 4 A, it is evident that a large numbers of FePt nanoparticles with an average size of ~3 nm (consistent well with the result of XRD) are uniformly distributed on the NC. Fig. 4 B reveals a high-resolution (HR) TEM image of FeS nanocrystals, which is magnified from the circle section in Fig. 4 A. The HR-TEM image shows distinct lattice fringes of FeS (101) planes with a spacing of 2.654 Å, as well as FeS (102) planes with a spacing of 2.092 Å. The inset shows the corresponding Fast Fourier Transform (FFT) of this

HR-TEM image, which suggests the same information of two planes. Fig. 4 C evinces the HR-TEM images of WC nanocrystals magnified from the square section in Fig. 4 A. Most significantly, all these WC nanocrystals indicate attractive 1D nanorod structures in diameter of 2 nm and length of 5 nm, which is close to the finding of XRD analysis. In addition, legible lattice fringes with a spacing of 2.526 Å, corresponding to that for the (100) facet of WC, are observed from Fig. 4 C. The TEM result above demonstrated that WC/FeS/FePt/NC hybrid electrocatalyst has been successfully achieved. The mass ratios of WC, FeS and Pt in the WC/FeS/FePt/NC sample have been determined by the ICP-AES technique, and the results are 19.4 wt %, 13.5 wt % and 21.6 wt %, respectively.

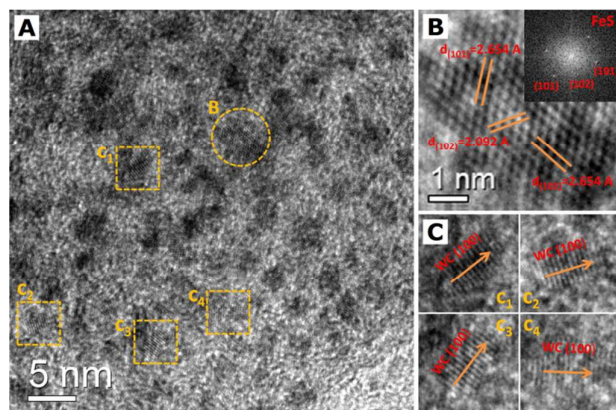


Fig. 4 Typical TEM images of the WC/FeS/FePt/NC sample: (A) the overall image and magnified images for (B) FeS and (C) WC.

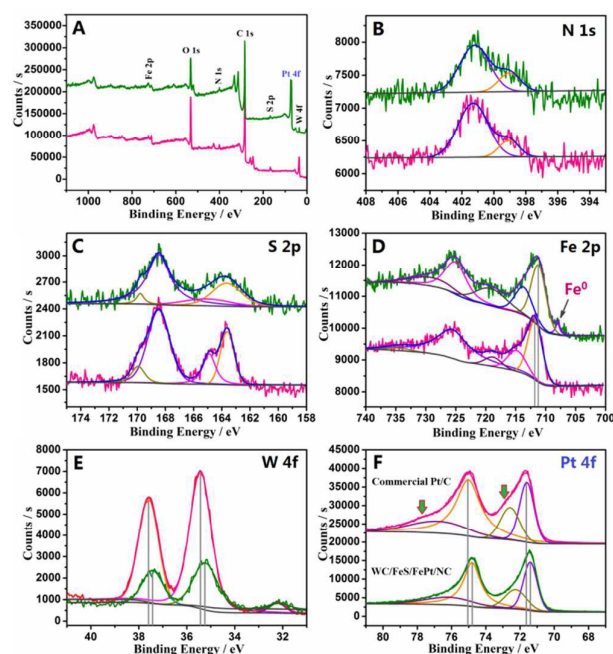


Fig. 5 XPS patterns the WC/FeS/NC (red) and WC/FeS/FePt/NC (green) samples: (A) the overall survey, (B) N 1s, (C) S 2p, (D) Fe 2p, (E) W 4f and (F) Pt 4f.

The XPS is also employed to elucidate the surface compositions and valence states of WC/FeS/NC and WC/FeS/FePt/NC samples, with the result shown in Fig. 5. The contents of different elements in

the two samples are summarized in Table 1. Obviously, several elements of C, O, N, S, Fe, and W are detected for WC/FeS/NC sample, and an added one of Pt is found for WC/FeS/FePt/NC sample (Fig. 5 A). The HR-XPS spectrum of N 1s peak (Fig. 5 B) reveals graphitic (401.2 eV) and pyridinic (398.9 eV) N species in the both samples.<sup>32</sup> The contents of N in the two samples are very similar (2.72 and 2.68 %), suggesting that the N species is well maintained after the introduction of Pt metal. From the S 2p spectrum (Fig. 5 C), it can be seen two main peaks at 163.7 and 168.5 eV, which are attributed to S<sup>2-</sup> and SO<sub>4</sub><sup>2-</sup>, respectively. Based on previous literatures<sup>33</sup>, a small amount of SO<sub>4</sub><sup>2-</sup> might be formed on the surface of metal sulfides, due to possible oxidation of S<sup>2-</sup> under the atmospheric environment. It is believed that the SO<sub>4</sub><sup>2-</sup> is formed only on the surface of FeS, and it can be dissolved in the aqueous solution. Therefore, the effect of SO<sub>4</sub><sup>2-</sup> on the ORR activity is negligible. The decreased S content (from 2.11% to 1.57%) after the formation of FePt alloy is largely due to the partial decomposition of FeS. The Fe 2p spectrum (Fig. 5 D) shows clear peaks of Fe 2p<sub>3/2</sub> and 2p<sub>1/2</sub> at 711.8 and 728.6 eV, respectively, suggesting the presence of a large portion of Fe<sup>2+</sup>.<sup>34</sup> After the fitting of peaks, the Fe 2p spectrum of WC/FeS/FePt/NC present slightly negative shift (0.55 eV) compared with that of WC/FeS/NC, and a new binding energy peak at 708 eV is observed that is attributed to the Fe<sup>0</sup> of FePt alloy.<sup>35</sup> Particularly, the almost equal contents of Fe for the two samples also indicate the Fe atom in FePt alloy would be originated from the FeS. The W 4f spectrum (Fig. 5 E) demonstrates that the peak intensity of W 4f is greatly reduced and peak position shifts to right with 0.2 eV after the introduction of Pt metal. The results originate from the fact that the WC nanorods are well surrounded by the FePt nanoparticles (as confirmed by TEM) and potential interface interaction between WC and FePt has been occurred. On the other hand, the contrastive Pt 4f spectrums of commercial Pt/C catalyst (TKK, 46.7% Pt) and WC/FeS/FePt/NC (21.6 % Pt) are further implemented (Fig. 5 F). The WC/FeS/FePt/NC exhibits a 0.2 eV decrease in binding energy compared to that of the commercial Pt/C, which is mainly due to the electron transfer from WC to metallic Pt (i.e. the electron-donating effect of carbide<sup>8</sup>), suggesting that the novel hybrid electrocatalyst is catalytically more active than the single Pt catalyst. Meanwhile, the Pt 4f spectrums also indicate a higher content of PtO (~46%) for the commercial Pt/C (see the arrows in Fig. 5 F for the Pt<sup>2+</sup> peak), while that of the WC/FeS/FePt/NC is only ~29%, which suggests a higher oxidation resistance of Pt for the present electrocatalysts.

Table 1 The contents (Atomic %) of different elements of the samples.

Samples	C	O	N	S	Fe	W	Pt
WC/FeS/NC	71.81	20.39	2.72	2.11	1.46	1.51	0.00
WC/FeS/FePt/NC	72.78	18.33	2.68	1.57	1.47	0.52	2.65

The ORR performances of the as-prepared electrocatalysts have been achieved in O<sub>2</sub>-saturated 0.1 M HClO<sub>4</sub> electrolyte by the RRDE methodology, with the results shown in Fig. 6. Fig. 6A displays the ORR curves at a scan rate of 5 mV s<sup>-1</sup> and a rotation rate of 1600 rpm. The FeS/NC exhibits obviously ORR catalytic activity with an onset potential of about 0.78 V. The current density is 3.27 mA cm<sup>-2</sup> at 0.6 V, and the diffusion-limited current density reaches 5.06 mA cm<sup>-2</sup> at 0.2 V. Remarkably, a more excellent ORR catalytic activity

is demonstrated for the WC/FeS/NC (with a higher onset potential of about 0.82 V). And higher current densities, 4.23 and 5.36 mA cm<sup>-2</sup>, are observed at 0.6 V and 0.2 V, respectively. Furthermore, the half-potential ( $E_{1/2}$ ) value of WC/FeS/NC is approximately 55 mV more positive than that of the FeS/NC, indicating that the introduction of WC reduces ORR overpotential effectively. The WC/FeS/FePt/NC (21.6 % Pt) electrocatalyst shows higher ORR catalytic activity than that of commercial Pt/C (TKK, 46.7% Pt) electrocatalyst in terms of the onset potential and  $E_{1/2}$ . The onset potentials are 1.03 V and 0.99 V for WC/FeS/FePt/NC and commercial Pt/C, respectively. The  $E_{1/2}$  values of WC/FeS/FePt/NC and Pt/C are 0.925 V and 0.890 V, respectively. The reduced overpotential of 35 mV is an evidence for the enhanced catalytic activity of WC/FeS/FePt/NC hybrid system. Fig. 6B reveals the mass activities based on Pt metals, which are calculated from the experimental data of ORR testing. Obviously, the Pt-mass activity at 0.9 V of the WC/FeS/FePt/NC is up to 317 mA mg<sup>-1</sup> Pt, which much higher than that of the commercial Pt/C (125 mA mg<sup>-1</sup> Pt). The measured activity of commercial Pt/C is in agreement with the reported values in previous literatures (100~130 mA mg<sup>-1</sup> Pt).<sup>36</sup> At the same time, the Pt-mass activities of previously reported alone WC-promoted Pt/C electrocatalysts are only 200~260 mA mg<sup>-1</sup> Pt.<sup>8-13</sup> Above results indicate that the additional promoting effect to Pt metal from the chalcogenide of FeS would be generated for the ORR, although the alloyed Fe and NC are considered to have some positive effects on the Pt-based electrocatalysts.<sup>22,25</sup> On the other hand, the ring currents (at constant 1.2 V) and relevant H<sub>2</sub>O<sub>2</sub> yields of these electrocatalysts are presented in Fig. 6C and Fig. 6D, respectively. The electron-transfer number “n” calculated from the ring currents at 0.4V are in the following order: WC/FeS/FePt/NC (3.997) > Pt/C (3.993) > WC/FeS/NC (3.980) > FeS/NC (3.967). Evidently, highly close four-electron processes are demonstrated for these electrocatalysts. And the H<sub>2</sub>O<sub>2</sub> yields are in the following order: WC/FeS/FePt/NC (0.13%) < WC/FeS/NC (1.02%) < FeS/NC (1.65%). The percentage of H<sub>2</sub>O<sub>2</sub> of the WC/FeS/FePt/NC is much lower than that of commercial Pt/C, which further proves the excellent ORR activity of the as-prepared hybrid electrocatalyst.

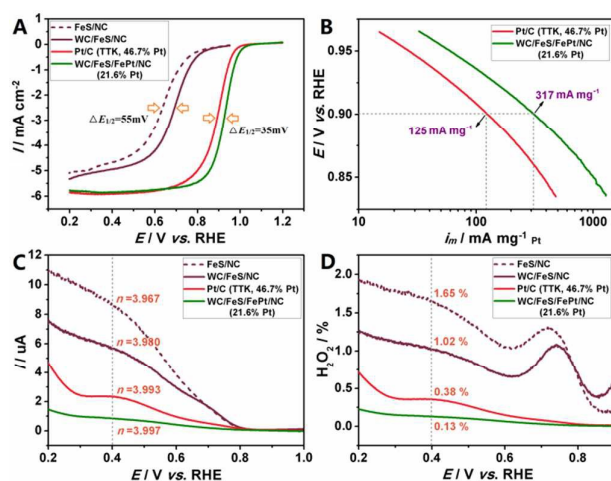


Fig. 6 Electrochemical performances of various electrocatalysts: (A) ORR curves, (B) mass activities, (C) ring current and (D) percentage of H<sub>2</sub>O<sub>2</sub>.

To further evaluate the catalytic activity of the WC/FeS/FePt/NC, the ORR curves of FeS/NC, WC/FeS/NC and WC/FeS/FePt/NC are collected at different rotating rates, with the results shown in Fig. 7. From Fig. 7 A-C, it can be clearly seen that the catalytic current densities increase with rotating rates for all these samples, which is in agreement with the reported results.<sup>24</sup> At every rotating rate, the current platform profiles of WC/FeS/NC are larger and steadier than those of the FeS/NC, indicating that the WC component is highly contributive to the efficient and steady performances for the ORR. Significantly, for all rotating rates, the current platform profiles of WC/FeS/FePt/NC reveal utterly steady and parallel characteristics ranging from 0.2 V to 0.8 V. The outstanding ORR performances for the WC/FeS/FePt/NC hybrid system are mainly attributed to the double promoting effects from WC and FeS components. Moreover, the catalytic mechanism of the ORR can be further analyzed with the Koutechy-Levich plot.<sup>37</sup> Fig. 7D displays the Koutechy-Levich plot at 0.4 V for the FeS/NC, WC/FeS/NC and WC/FeS/FePt/NC. These plots show linear lines which are fairly parallel to the theoretical line of the four-electron reduction mechanism, strongly indicative of the four-electron process for the present electrocatalysts.

With regard to the improvement of ORR catalytic activity for the WC/FeS/FePt/NC electrocatalyst, several possible reasons have been summarized as follows. Firstly, WC as a promoter might provide a main promoting effect to the catalytic activity of Pt metal, which is attributed to the electron-donating effect of carbides and changes in electronic structure of Pt metal.<sup>8</sup> Secondly, FeS as a non-precious metal catalyst exhibits obviously ORR catalytic activity in acidic electrolyte,<sup>18</sup> which is expected to strengthen catalytic efficiency for Pt metal in some sense. Thirdly, the introduction of WC has effectively enhanced the catalytic activity for the FeS, which suggests the double promoting effects on Pt metal from WC and FeS components might be in operation for the WC/FeS/FePt/NC system. Meanwhile, the hybrid architecture of FePt alloys and nitrogen-doped carbon also plays a fundamental role on the improvements of ORR performance relative to Pt/C catalyst, due to their alloying effects and synergistic effects.<sup>22,25</sup> More controlled experiments and detailed discussions are in progress.

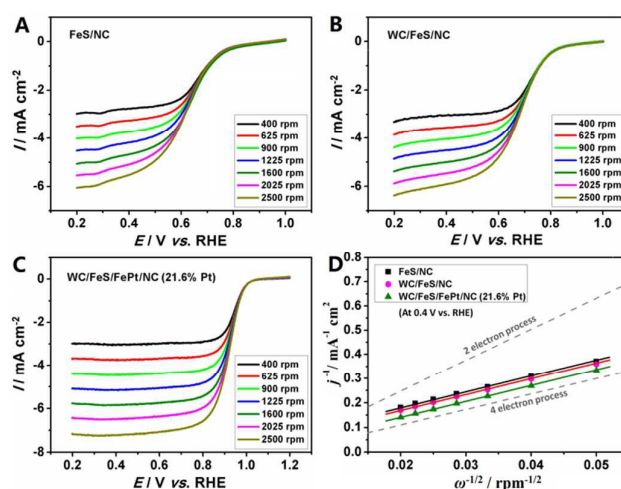


Fig. 7 ORR curves of (A) FeS/NC, (B) WC/FeS/NC and (C) WC/FeS/FePt/NC electrocatalysts at different rotating rates (from 400 to 2500 rpm) with the same scan rate of 5 mV s<sup>-1</sup>. (d) The Koutechy-Levich plots for ORR at 0.4 V.

The durability of WC/FeS/FePt/NC electrocatalysts with respect to commercial Pt/C is investigated through the chronoamperometry measurements in O<sub>2</sub>-saturated 0.1 M HClO<sub>4</sub> electrolyte at a rotation rate of 1600 rpm (see Fig. 8). Fig. 8 A and B show the corresponding chronoamperometric curves of the electrocatalysts at 0.4 V and 0.8 V, respectively. As revealed from Fig. 8 A, the current-time (i-t) chronoamperometric response for the WC/FeS/NC exhibits a very slow attenuation with high current retention (86.7%) after 18000 s. The result indicates that, as the attractive promoting components, the WC/FeS/NC possesses excellent electrocatalytic stability in the acidic electrolyte, which would endow with a persistent high activity for the WC/FeS/FePt/NC electrocatalysts. Actually, the experimental results prove that WC/FeS/FePt/NC exhibits a superior durability to Pt/C at 0.4 V, with the current retention of 61.8% and 56.3%, respectively. Remarkably, the WC/FeS/FePt/NC still demonstrates an outstanding stability with a current retention of 52.4% at the high potential of 0.8 V, while that of the Pt/C is only 33.5% (Fig. 8 B), suggesting its superior electrocatalytic stability of our electrocatalyst towards ORR under the rigorous oxidizing condition.

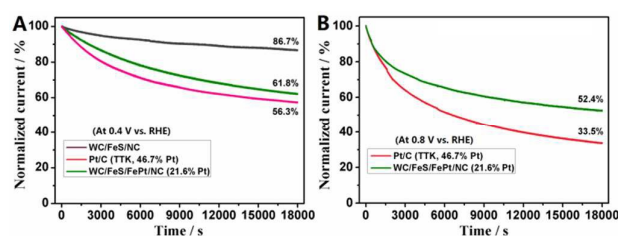


Fig. 8 chronoamperometric curves (under the rotation rate of 1600 rpm) of the electrocatalysts at different potential: (A) 0.4 V and (B) 0.8 V.

## Conclusions

In summary, a novel WC/FeS/FePt/NC hybrid architecture has been successfully synthesized via an efficient ion-exchange and sintering associated strategy. Structural analysis shows that the unique 1D WC nanorods with ultrafine structure are achieved and the FePt alloy is formed by the in-situ growth from FeS nanocrystals. As a Pt-free catalysts, the FeS/NC exhibits obviously ORR catalytic activity with an onset potential of 0.78 V. And the WC/FeS/NC behaves a more excellent activity to ORR with a higher onset potential of 0.82 V, because of enhancement of WC. Owing to the collective promoting effects from WC and FeS components, much higher catalytic activity and stability of the WC/FeS/FePt/NC have been demonstrated for the ORR, comparing with commercial Pt/C. It is highly expected that design and synthesis of multi-component hybrid architectures (e.g. carbides and sulphides) is a promising route to fabricate high-performance Pt-based electrocatalysts with lower Pt loading, so as to significantly reduce the cost of fuel cell systems.

## Acknowledgements

Financial support by the National Natural Science Foundation of China (21443006), Provincial Natural Science Foundation of Guangdong (2014A030310179), Young Creative Talents Project of Guangdong Province Education Department (2014KQNCX200), Science and Technology Project of Maoming (2014006) and Doctor

Startup Project of the local University (513086) are gratefully acknowledged.

## Notes and references

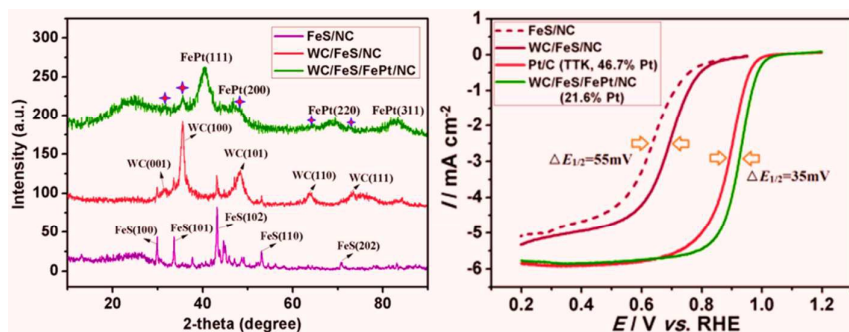
- (a) Y. Wang, J. Qiao, R. Baker, J. Zhang, *Chem. Soc. Rev.*, 2013, **42**, 5768-5787. (b) S. Zhang, Y. Shao, G. Yin, Y. Lin, *J. Mater. Chem. A*, 2013, **1**, 4631-4641.
- (a) Z. Li, Y. Li, S.P. Jiang, G. He, P.K. Shen, *J. Mater. Chem. A*, 2014, **2**, 16898-16904. (b) W. Yuan, S. Lu, Y. Xiang, S.P. Jiang, *RSC Adv.*, 2014, **4**, 46265-46284.
- (a) C. Zhang, S.Y. Hwang, Z. Peng, *J. Mater. Chem. A*, 2014, **2**, 19778-19787. (b) B.A. Kakade, H. Wang, T. Tamaki, H. Ohashi, T. Yamaguchi, *RSC Adv.*, 2013, **3**, 10487-10496.
- (a) X. Li, X. Li, M. Xu, J. Xu, H. Chen, *J. Mater. Chem. A*, 2014, **2**, 1697-1703. (b) S.M. Unni, V.K. Pillai, S. Kurungot, *RSC Adv.*, 2013, **3**, 6913-6921.
- (a) X. Tian, J. Luo, H. Nan, Z. Fu, J. Zeng, S. Liao, *J. Mater. Chem. A*, 2015, **3**, 16801-16809. (b) L. Zhang, J. Kim, E. Dy, S. Ban, K. Tsay, H. Kawai, Z. Shi, J. Zhang, *Electrochim. Acta*, 2013, **108**, 480-485.
- (a) A. Morozan, B. Josselme, S. Palacin, *Energy Environ. Sci.*, 2011, **4**, 1238-1254. (b) X. Ding, S. Yin, K. An, L. Luo, N. Shi, Y. Qiang, S. Pasupathi, B.G. Pollet, P.K. Shen, *J. Mater. Chem. A*, 2015, **3**, 4462-4469.
- (a) S. Yin, M. Cai, C. Wang, P.K. Shen, *Energy Environ. Sci.*, 2011, **4**, 558-563. (b) Z. Hu, C. Chen, H. Meng, R. Wang, P.K. Shen, H. Fu, *Electrochem. Commun.*, 2011, **13**, 763-765. (c) Z. Yan, G. He, P.K. Shen, Z. Luo, J. Xie, M. Chen, *J. Mater. Chem. A*, 2014, **2**, 4014-4022. (c) Z. Li, S. Ji, B.G. Pollet, P.K. Shen, *Chem. Commun.*, 2014, **50**, 566-568.
- (a) Z. Yan, G. He, M. Cai, H. Meng, P.K. Shen, *J. Power Sources*, 2013, **242**, 817-823. (b) G. Cui, P.K. Shen, H. Meng, J. Zhao, G. Wu, *J. Power Sources*, 2011, **196**, 6125-6130.
- X. Zhou, Y. Qiu, J. Yu, J. Yin, S. Gao, *Int. J. Hydrogen Energ.*, 2011, **36**, 7398-7404.
- C.K. Poh, S.H. Lim, Z. Tian, L. Lai, Y.P. Feng, Z. Shen, J. Lin, *Nano Energy*, 2013, **2**, 28-39.
- He, H. Meng, X. Yao, P.K. Shen, *Int. J. Hydrogen Energ.*, 2012, **37**, 8154-8160.
- Z. Yan, M. Cai, P. K. Shen, *Scientific Reports*, 2013, **3**, 1646.
- G. He, Z. Yan, X. Ma, H. Meng, P.K. Shen, C. Wang, *Nanoscale*, 2011, **3**, 3578-3582.
- M. Gao, Y. Xu, J. Jiang, S.H. Yu, *Chem. Soc. Rev.*, 2013, **42**, 2986-3017.
- M. Gao, J. Jiang, S.H. Yu, *Small*, 2012, **8**, 13-27.
- R.A. Sidk, A.B. Anderson, *J. Phys. Chem. B*, 2006, **110**, 936-941.
- M. Gao, W. Yao, H. Yao, S.H. Yu, *J. Am. Chem. Soc.*, 2009, **131**, 7486-7487.
- (a) D. Susac, A. Sode, L. Zhu, P. Wong, M. Teo, D. Bizzotto, K. A. R. Mitchell, R. R. Parsons, S.A. Campbell, *J. Phys. Chem. B*, 2006, **110**, 10762-10770. (b) D. Susac, L. Zhu, M. Teo, A. Sode, K. C. Wong, P.C. Wong, R.P. Parsons, D. Bizzotto, K.A.R. Mitchell, S. A. Campbell, *J. Phys. Chem. C*, 2007, **111**, 18715-18723.
- Z. Yan, J. Xie, S. Zong, M. Zhang, Q. Sun, M. Chen, *Electrochim. Acta*, 2013, **109**, 256-261.
- (a) M. R. Gao, S. Liu, J. Jiang, C. H. Cui, W. T. Yao, S.H. Yu, *J. Mater. Chem.*, 2010, **20**, 9355-9361. (b) M. Gao, Q. Gao, J. Jiang, C. Cui, W. Yao, S.H. Yu, *Angew. Chem. Int. Ed.*, 2011, **50**, 4905-4908.
- J. Wu, P. Li, Y. Pan, S. Warren, X. Yin, H. Yang, *Chem. Soc. Rev.*, 2012, **41**, 8066-8074.
- J. Kim, Y. Lee, S. Sun, *J. Am. Chem. Soc.*, 2010, **132**, 4996-4997.
- H. Huang, X. Wang, *J. Mater. Chem. A*, 2014, **2**, 6266-6291.
- (a) Z. Wu, S. Yang, Y. Sun, K. Parvez, X. Feng, K. Mullen, *J. Am. Chem. Soc.*, 2012, **134**, 9082-9085. (b) Y. Liang, Y. Li, H. Wang, J. Zhou, J. Wang, T. Regier, H. Dai, *Nat. Mater.*, 2011, **10**, 780-786.
- (a) B. Zheng, J. Wang, F. Wang, X. Xia, *J. Mater. Chem. A*, 2014, **2**, 9079-9084. (b) K. Jukk, N. Kongi, L. Matisen, T. Kallio, K. Kontturi, K. Tammeveski, *Electrochim. Acta*, 2014, **137**, 206-212.
- Z. Guo, H. Zhang, B. Han, W. Yuan, *Physica C*, 2015, **509**, 29-33.
- A. Hassan, V.A. Paganin, E.A. Ticianelli, *Appl. Catal. B-Environ.*, 2015, **165**, 611-619.

## Journal Name

## ARTICLE

- 28 (a) N. Matsuda, T. Nakashima, T. Kato, H. Shiroishi, *Electrochim. Acta*, 2014, **146**, 73-78. (b) S. Shanmugam, J. Sanetuntikul, T. Momma, T. Osaka, *Electrochim. Acta*, 2014, **137**, 41-48.
- 29 D. Wang, Y. Li, *Inorg. Chem.*, 2011, **50**, 5196-5202.
- 30 (a) Q. Pang, S. Yang, C. Ge, Y. Liu, X. Liu, Y. Fang, J. Zhou, Z. Li, L. Zhou, *Electrochim. Acta*, 2013, **114**, 334-340. (b) S. Meenakshi, K.G. Nishanth, P. Sridhar, S. Pitchumani, *Electrochim. Acta*, 2014, **135**, 52-59.
- 31 S. Yang, C. Zhao, C. Ge, X. Dong, X. Liu, Y. Liu, Y. Fang, H. Wang, Z. Li, *J. Mater. Chem.*, 2012, **22**, 7104-7107.
- 32 H. Zhang, Y. Wang, D. Wan, Y. Li, X. Liu, P. Liu, H. Yang, T. An, Z. Tang, H. Zhao, *Small*, 2014, **10**, 3371-3378.
- 33 (a) H. Geng, L. Zhu, W. Li, H. Liu, L. Quan, F. Xi, X. Su, *J. Power Sources*, 2015, **281**, 204-210. (b) W. Cao, L. Chen, Z. Qi, *Catal. Lett.*, 2014, **144**, 598-606.
- 34 H. Chen, L. Zhu, H. Liu, W. Li, *J. Power Sources*, 2014, **245**, 406-410.
- 35 D. Chen, X. Zhao, S. Chen, H. Li, X. Fu, Q. Wu, *Carbon*, 2014, **68**, 755-762.
- 36 Y. Nie, L. Li, Z. Wei, *Chem. Soc. Rev.*, 2015, **44**, 2168-2201.
- 37 Y. Wu, Q. Shi, Y. Li, Z. Lai, H. Yu, H. Wang, F. Peng, *J. Mater. Chem. A*, 2015, **3**, 1142-1151.

## Graphic abstract



Novel multi-component WC/FeS/FePt/NC electrocatalysts with excellent mass activity and superior durability are developed for the oxygen reduction reaction in fuel cells.